



*Citation for published version:*

Henderson, J-P, Plummer, A & Johnston, N 2018, 'An electro-hydrostatic actuator for hybrid active-passive vibration isolation', *International Journal of Hydromechatronics*, vol. 1, no. 1, pp. 47-71.  
<https://doi.org/10.1504/IJHM.2018.090305>

*DOI:*

[10.1504/IJHM.2018.090305](https://doi.org/10.1504/IJHM.2018.090305)

*Publication date:*

2018

*Document Version*

Peer reviewed version

[Link to publication](#)

## University of Bath

### General rights

Copyright and moral rights for the publications made accessible in the public portal are retained by the authors and/or other copyright owners and it is a condition of accessing publications that users recognise and abide by the legal requirements associated with these rights.

### Take down policy

If you believe that this document breaches copyright please contact us providing details, and we will remove access to the work immediately and investigate your claim.

# An electro-hydrostatic actuator for hybrid active-passive vibration isolation

**Jean-Paul HENDERSON, Andrew PLUMMER, Nigel JOHNSTON**

Centre for Power Transmission and Motion Control, Department of Mechanical Engineering, University of Bath, UK. A.R.Plummer@bath.ac.uk

## **ABSTRACT**

The concept, design, modelling and testing of a novel electro-hydrostatic actuator (EHA) intended for active vibration isolation is described. The EHA consists of a brushless DC motor integrated with a bidirectional gear pump, controlling oil flow to a double-ended hydraulic cylinder. The permanent magnet rotor runs in oil, the motor and pump forming a pressure vessel pre-charged to a mean system pressure (about 80 bar). This arrangement means no pump case drain and refeeding circuit is required. The actuator is designed to cancel the force transmitted through a flexible vibration mount, with dominant vibration frequency of around 20Hz. The particular motivation is to provide isolation between a helicopter fuselage and the vibrating rotor hub, and would be integrated into the flexible strut connecting the two. The inertia of the EHA is tuned to provide a degree of passive vibration isolation at the dominant frequency, and hence is termed a Resonant EHA. Active control of the motor extends the isolation performance of the passive device by compensating for losses (which give damping), and extend the frequency of isolation away from the resonant frequency. A 7kN prototype has been built and extensively tested, demonstrating a reduction by a factor of four in the root-mean-square transmitted force and a near elimination at the fundamental frequency. The advantage of the Resonant EHA is a wider range of operating frequencies than a purely passive system, and a lower power consumption than a purely active system.

## **KEYWORDS**

EHA, tuned mass damper, rotorcraft, vibration isolation, inerter

## **1. INTRODUCTION**

An electro-hydrostatic actuator (EHA) incorporates a hydraulic pump to transform the rotational motion of an electric servomotor to the linear motion of a piston by means of fluid under pressure. The piston motion is controlled via angular motion control of the motor. The ratio of piston area to pump displacement determines the gear ratio. An EHA is a more energy efficient actuator than a servovalve-controlled hydraulic cylinder due to the absence of valve throttling losses.

EHAs have been developed for aerospace applications for several decades. An experimental EHA for use in the aileron of an F-18 aircraft was described [1]. It was noted that compared to a servovalve-controlled actuator, the dynamic performance was inferior due to the acceleration limitations of the motor. The development of EHAs for the Airbus A380 is outlined in [2]. An increasing number of ground-based industrial applications are now emerging. Six EHAs forming a flight simulator motion system are described in [3], where a 90% power saving compared to the conventional servovalve-controlled system is reported.

In this paper we describe and investigate an EHA developed for vibration isolation. Required operating frequencies are around 20Hz, necessitating a higher dynamic performance than many existing EHAs. However the servomotor inertia, which is normally the main dynamic limitation, can be used to advantage by providing some passive isolation in the manner of a tuned mass damper.

### **1.1 Motivation**

This research is relevant to general vibration isolation problems, but a specific motivation is the need for vibration isolation between the rotor hub and fuselage in helicopters. Oscillating forces are generated when a helicopter's rotor blades pass through the relative airstream present during forward flight. These forces cause rotor hub vibration which should be isolated from the fuselage to increase structural lifetime, and prevent pilot and passenger fatigue. The vibration has a dominant frequency, the blade passing frequency, which is typically around 20Hz. A small variation in the frequency is expected in future variable rotor speed systems.

The Active Control of Structural Response (ACSR) vibration suppression system has been used successfully for many years in large helicopters [4]. As shown in Figure 1, it uses four compliant glass-fibre composite struts between rotor hub and fuselage, and a hydraulic actuator in each strut to dynamically extend the strut to accommodate the vibration of the rotor hub without the need for dynamic force transmission to the fuselage. The struts are sufficiently stiff to transmit static loads without excessive extension. The actuators are controlled via an adaptive scheme which

minimizes measured fuselage acceleration. However it is inconvenient to provide a hydraulic connection to each strut, and a more energy efficient electrically-powered actuation method is sought which might also be suitable for smaller helicopters. Note that an additional requirement is that any actuation system should be sufficiently robust to survive impact forces during emergency landing.

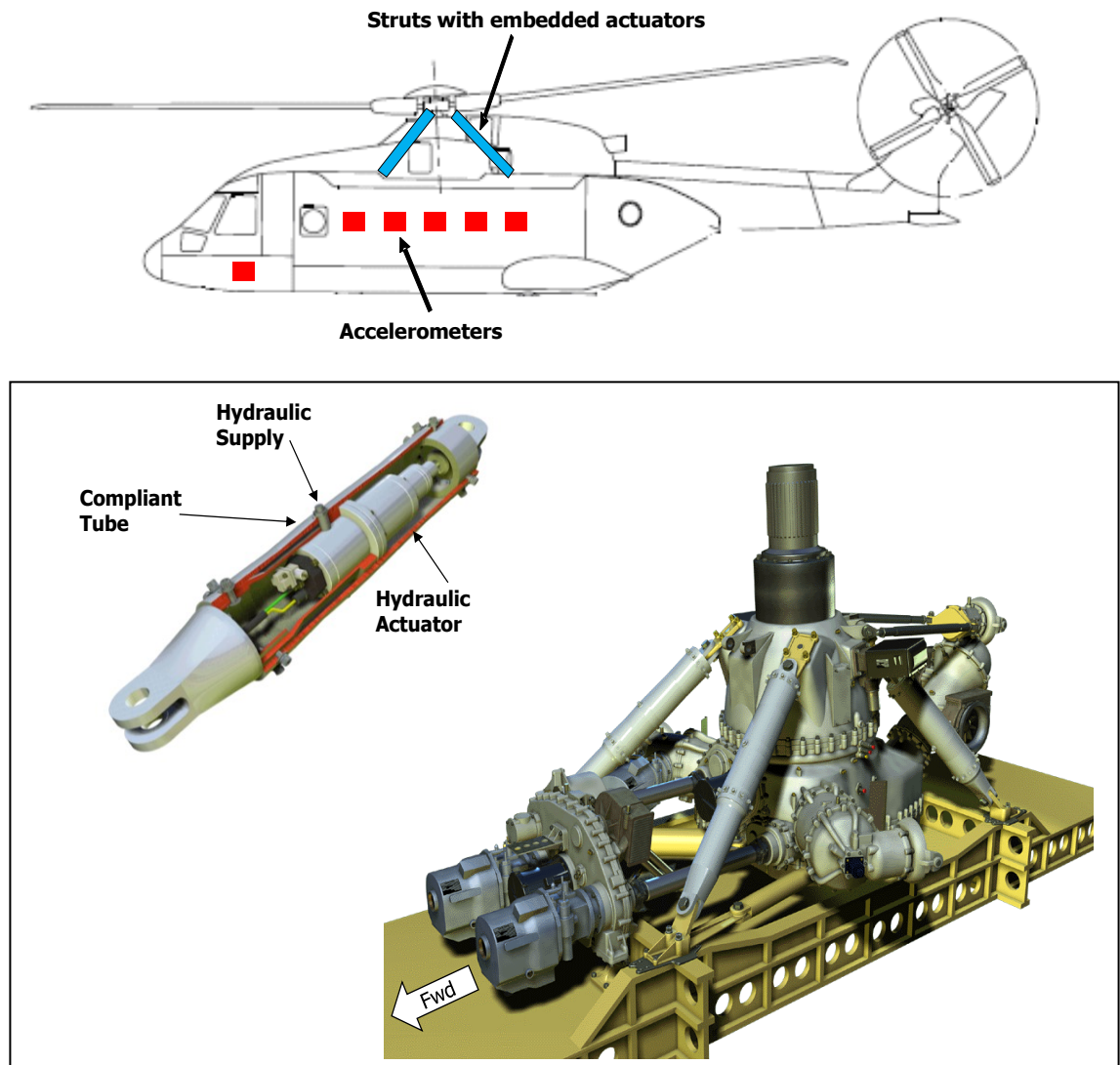


Figure 1. Existing ACSR vibration isolation system: single strut cutaway showing hydraulic actuator (left), and rotor hub with four struts connecting to fuselage below (top and right).

Images courtesy Leonardo.

A single actuator acting in parallel with a 20 kN/mm stiffness strut would need to exhibit the following characteristics:

- $\pm 7$  kN force
- $\pm 350$   $\mu\text{m}$  dynamic stroke at dominant frequency
- 20 Hz dominant frequency, with minus 10% frequency change potential
- $\pm 2$  mm low frequency displacement change (strut deflection due to lift force variation)

## 1.2 Passive vibration isolation

ACSR is a fully active vibration control system. In contrast, passive vibration isolation systems require no external power. DAVI (Dynamic Anti-Resonant Vibration Absorber) and SARIB (Système Antivibratoire à Résonateur Intègre à Barres) are examples of helicopter tuned-mass vibration absorbers in which a mass on the end of a pivoted lever arm is sized to interact with a support stiffness so that the inertia force cancels the stiffness force. This is shown in Figure 2, in which  $x$  is the displacement of the vibrating component, and the requirement is to minimize the resultant force transmitted to ground. The pivoted lever arm gives a gearing ratio that makes the differential inertia larger than the mass by a factor of the gearing ratio squared. A mass spun by a ballscrew is another way of achieving a high differential inertia, and such a device termed an “inertor” [5] has been implemented in Formula 1 motor racing as a suspension element. The inertor is more compact than the lever-based devices, and is less susceptible to stroke saturation. The use of fluid inertance as the resonating mass is the idea behind the Liquid Isolation Vibration Eliminator (LIVE) [6], which has been used successfully. For the LIVE system there is a hydraulic gearing mechanism due to the difference in area between the driven piston and the tube which contains the resonating fluid. The Anti-Resonance Isolation System (ARIS) is also based on hydraulic principles and has been implemented commercially by Eurocopter [7].

Passive vibration isolation systems have the disadvantage of being tuned to one specific frequency. Variable (or adaptable) passive systems are more flexible with respect to long term variation in conditions by allowing real time tuning of the device. The addition of an actuator that changes the location of a mass, and therefore the effective inertia of a tuned mass system is one example of a variable passive system as shown in [8].

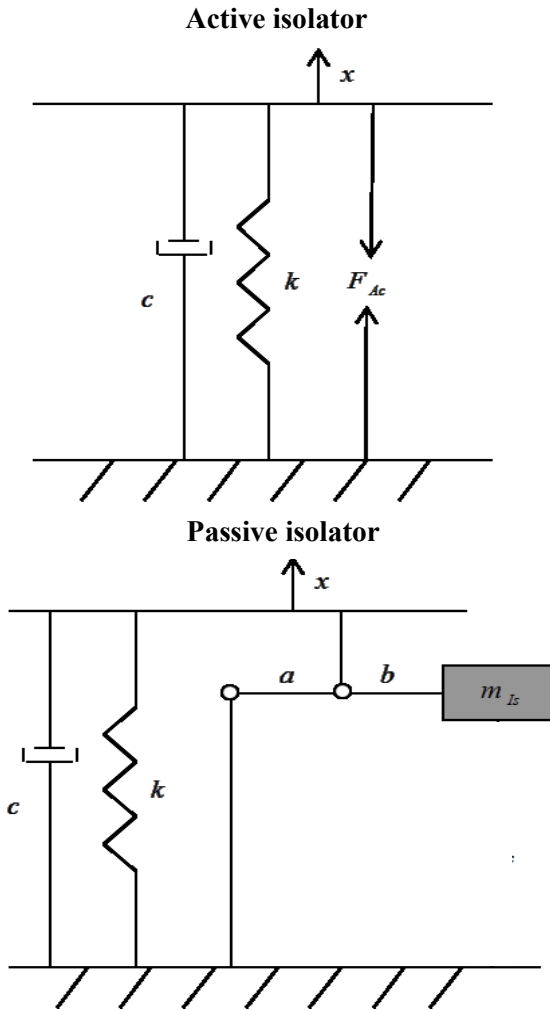


Figure 2. Top: active vibration isolator using actuator force  $F_{Ac}$ .  
 Bottom: passive tuned mass isolator

### 1.3 Hybrid Active-Passive isolation

Figure 3 shows an actuator augmenting the force of a resonating mass, forming a hybrid system. For the helicopter application each strut can be treated separately, so  $x$  is the displacement of the rotor hub resolved along the strut axis,  $c$  is the damping of the strut lumped with losses in the actuator, and  $k$  is the strut stiffness. The lengths  $a$  and  $b$  determine a linear mechanical gearing ratio for the mass  $m_{Is}$ . The advantage of including an actuator is to be able to extend the range of the passive isolation, both in terms of broadening the frequency band and cancelling the damping force. This can be achieved with lower actuator force and power compared to a purely active system, assuming the operating frequency is not too far from the design point of the passive system.

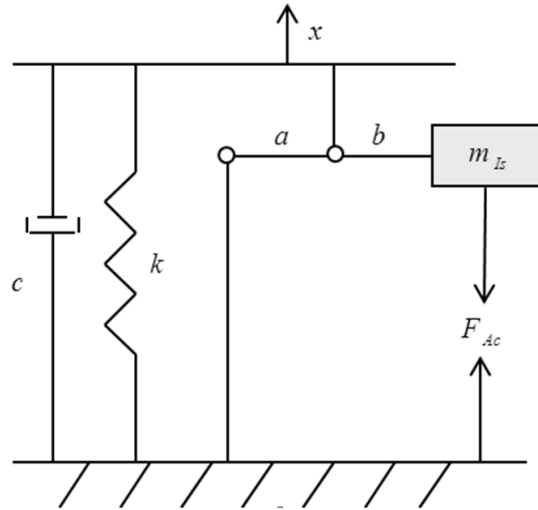


Figure 3. Hybrid active-passive isolator formed by adding actuator force  $F_{Ac}$  to tuned mass damper

Non-gearred actuated reaction mass isolators for space applications are presented in [9]. Incorporating passive isolation is shown to give lower actuator power. The use of a “Smart Spring” with an electromagnet to actively isolate marine machinery in parallel with passive elements is described in [10]. Hybrid hydraulic engine mounts which include active assistance from solenoid actuators have been reviewed in [11]. In each engine mount the fluid is the resonating element but the addition of the actuator gives the ability to tailor the vibration response to specific driving or load conditions [12].

Theoretical research on a semi-active hydraulic vibration isolator has recently been published [13], which suggests the use of displaced fluid from a hydraulic cylinder to drive a hydraulic motor attached to a flywheel. This ‘inertor’ can be made semi-active by varying the flywheel inertia.

### 1.3 An EHA as a hybrid isolator

An appropriately sized EHA placed in parallel with a support spring naturally forms a hybrid active-passive vibration isolator. The dominant inertia is that of the servomotor rotor, and the gear ratio dictated by pump displacement and piston area can be chosen to give a large inertor value, i.e. a large EHA force in proportion to the relative acceleration across the EHA. Torque control of the servomotor provides the active element. In the helicopter example, the strut forms

the parallel spring stiffness, and the inerter value should be chosen to cancel the strut force at the blade passing frequency (i.e. this is the resonant frequency of the isolator). The advantages of using the EHA hybrid isolator for this application include:

- Compared to an active system, a hybrid system will reduce the power requirement of the actuator if operating near the passive isolation frequency, and so minimise the heat generated in the strut.
- A life of about 700 million cycles is required, which would be challenging to achieve with a mechanical gearing system as opposed to a hydraulic one.
- The cross-line pressure in the EHA can be limited by relief valves to protect the actuator in the case of a sudden impact due to emergency landing. This would be hard to do with a purely mechanical system.

#### **1.4 Paper structure**

In the remainder of this paper, first the concept of the ‘Resonant EHA’ for vibration isolation is analysed using simple linear models. Then the design and construction of a proof-of-principle prototype are described, along with test results which help to characterize its behaviour. The development of a non-linear simulation model is presented, including estimation of some parameter values based on experimental data. Finally experimental results are presented, compared with simulation, and an assessment of vibration isolation performance made. More detail on many of these aspects can be found in the PhD thesis of Henderson [14].

## **2 CONCEPT AND LINEAR ANALYSIS**

### **2.1 Resonant EHA concept**

Figure 4 shows the resonant EHA schematic. The servomotor driven pump is directly connected to a double-ended hydraulic cylinder which is mounted in parallel to a spring. Relief valves limit the pressure difference between the hydraulic lines, but are normally expected to be closed. The minimum pressure is dictated by an accumulator which is connected to the case drain of the pump, and also connects to the servomotor housing so that the motor rotor runs in fluid; this arrangement is discussed in Section 3.



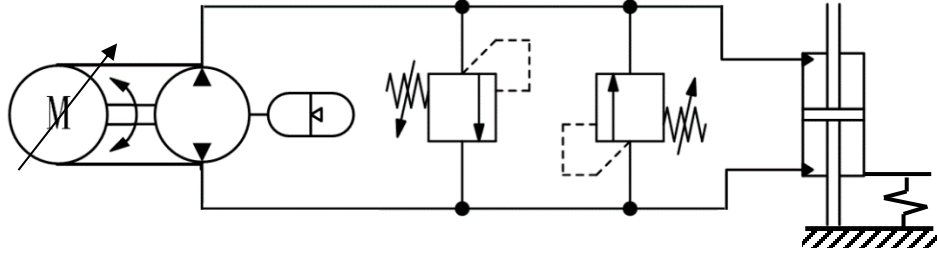


Figure 4. Resonant EHA hydraulic diagram.

A linear model of the Resonant EHA can be developed by reference to the mechanical analogy in Figure 5. This is the same as Figure 3 with the addition of spring  $k_{Eq}$  which represents a transmission stiffness due to the compressibility of the hydraulic fluid. It is important to understand the effect of the compressibility as this constitutes a deviation away from the ideal characteristic.

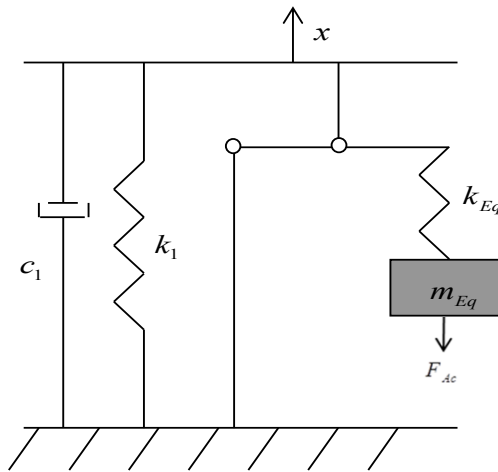


Figure 5 Linear mechanical analogy of Resonant EHA

## 2.2 Linear dynamic analysis

The steady-state ‘gearing’ which converts between linear and rotary velocity is given by:

$$\dot{\theta} = \frac{A}{D} \dot{x} \quad (1)$$

where  $x$  is linear EHA displacement,  $\theta$  is pump angle,  $A$  is the area of the piston, and  $D$  is the volumetric displacement of the pump.

The sum of forces on the fuselage as a function of the linear displacement  $x$  and pump angle  $\theta$  is:

$$c_1 \dot{x} + kx + \frac{A}{D} \left( k_2 \left( \frac{A}{D} x - \theta \right) \right) = F_{Fu} \quad (2)$$

where  $c_1$  is any damping parallel to the strut,  $k$  is the strut stiffness and  $k_2$  is the pump torsional stiffness given by:

$$k_2 = \frac{2BD^2}{V_{To}} \quad (3)$$

and where  $V_{To}$  is the total of volume of fluid between the pump and piston on one side of the pump, and  $B$  is the effective fluid bulk modulus. The equation of motion for the motor rotor and pump is:

$$k_2 \left( \frac{A}{D} x - \theta \right) - T_{Mo} = I \ddot{\theta} + c_2 \dot{\theta} \quad (4)$$

where  $T_{Mo}$  is the motor torque,  $I$  is the combined motor and pump inertia, and  $c_2$  is the torsional damping of the pump and motor. Using Equation (4) to substitute for  $\theta$  in Equation (2) and transforming to the Laplace domain gives:

$$F_{Fu}(s) = \left( \left( \frac{A}{D} \right)^2 \frac{k_2(Is^2 + c_2s)}{Is^2 + c_2s + k_2} + c_1s + k \right) X(s) + \left( \frac{A}{D} \right) \frac{k_2}{Is^2 + c_2s + k_2} T_{Mo}(s) \quad (5)$$

The transfer function of motor torque over rotor displacement for obtaining zero net force on the fuselage is:

$$\frac{T_{Mo}(s)}{X(s)} = -\frac{D}{A} \left( \frac{c_1I}{k_2} s^3 + \left( \left( \frac{A}{D} \right)^2 I + \frac{c_2c_1}{k_2} + \frac{k_1I}{k_2} \right) s^2 + \left( \frac{c_2k_1}{k_2} + c_1 + c_2 \left( \frac{A}{D} \right)^2 \right) s + k \right) \quad (6)$$

And the transfer function for passive force transmission, i.e. setting the motor torque to zero in Equation (5), is:

$$\frac{F_{Fu}(s)}{X(s)} = \left( \frac{A}{D} \right)^2 \frac{k_2(Is^2 + c_2s)}{Is^2 + c_2s + k_2} + c_1s + k \quad (7)$$

When  $k_2$  goes to infinity giving the ideal case of zero transmission compliance, equations (5) and (6) become, respectively:

$$\frac{T_{Mo}(s)}{X(s)} = -\frac{D}{A} \left( \left( \frac{A}{D} \right)^2 Is^2 + cs + k \right) \quad (8)$$

$$\frac{F_{Fu}(s)}{X(s)} = \left(\frac{A}{D}\right)^2 Is^2 + cs + k \quad (9)$$

where  $c$  is the combined strut and pump-motor damping. In the frequency domain, equations (8) and (9) become (respectively):

$$\frac{T_{Mo}(j\omega)}{X(j\omega)} = -\frac{D}{A} \left( k - \left(\frac{A}{D}\right)^2 I\omega^2 + jc\omega \right) \quad (10)$$

$$\frac{F_{Fu}(j\omega)}{X(j\omega)} = k - \left(\frac{A}{D}\right)^2 I\omega^2 + jc\omega \quad (11)$$

The natural frequency, i.e. the frequency at which the inertial and spring forces are in anti-phase and so the real part in equation (11) becomes zero, is given by:

$$\omega_n = \frac{D}{A} \sqrt{\frac{k}{I}} \quad (12)$$

This equation is consistent with an equivalent mass  $m_{Eq}$ , i.e. the motor-pump inertia referred to the linear motion of the EHA, given by:

$$m_{Eq} = \frac{A^2}{D^2} I \quad (13)$$

As expected, the inertia is scaled by the square of the gear ratio given by equation (1).

As is well known for second order systems, the transmitted force in equation (11) is actually at a minimum at the resonant frequency, given by:

$$\omega_r = \omega_n \sqrt{1 - 2\zeta^2} \quad (14)$$

where  $\zeta$  is the damping ratio given by  $\frac{c}{2\sqrt{km_{Eq}}}$ . The natural frequency and resonant frequency

are very similar for damping ratios much smaller than one.

### 2.3 The effect of Transmission Compliance

From Equation (10) it can be seen that at the natural frequency, the torque required for zero transmitted force is a function only of the damping, i.e. losses, in the device. Figure 6 shows a Bode plot for this transfer function, using the example parameters in Table 1. The natural frequency is 26Hz, damping ratio is 0.25, and the resonant frequency is 24Hz. For the helicopter vibration isolation application, a displacement amplitude of 0.35 mm is expected, requiring a 1.9

Nm torque amplitude if the vibration frequency is in the range 90%-100% of the natural frequency (consistent with the specification in Section 1.1). . Figure 6 also shows the required torque Bode plot when the transmission compliance is non-zero, generated used Equation (6). A 900 MPa fluid bulk modulus  $B$  is assumed with a fluid volume  $V_{T_o}$  of 8.9 cm<sup>3</sup>, from which Equation (3) gives the transmission stiffness as stated in Table 1. This is equivalent to a linear stiffness at the EHA output of 61 kN/mm. The Figure shows that the transmission compliance lowers the minimum torque frequency but the torque magnitude is similar to the infinite bulk modulus curve.

Table 1 Example parameters

Parameter		Value
Piston area	$A$	550 mm <sup>2</sup>
Pump displacement	$D$	1.5 cm <sup>3</sup> /rev
Motor-pump inertia	$I$	1.4x10 <sup>-4</sup> kgm <sup>2</sup>
Damping	$c$	60 kNs/m
Strut stiffness	$k$	20 kN/mm
Torsional transmission stiffness	$k_2$	11.6 Nm/rad

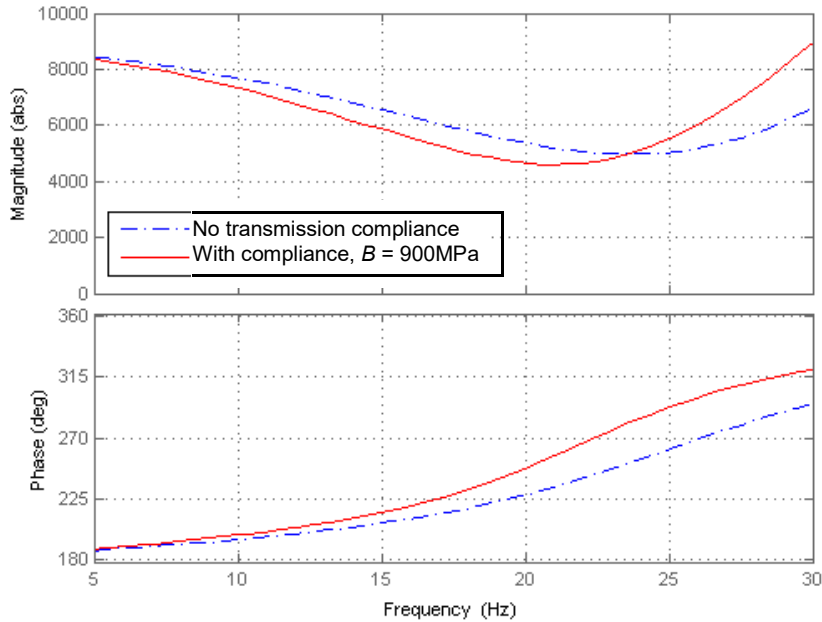


Figure 6. Required torque per vibration displacement (Nm/m) transfer function

The passive vibration transmission characteristics from Equations 7 and 9 up to 100 Hz are shown in Figure 7. Without transmission compliance the transmitted force rises with frequency monotonically. With transmission compliance there is a distinct peak. Thus there is a danger of high frequency vibration components being amplified, such as a harmonic of the lower frequency fundamental input which may coincide with the peak frequency.

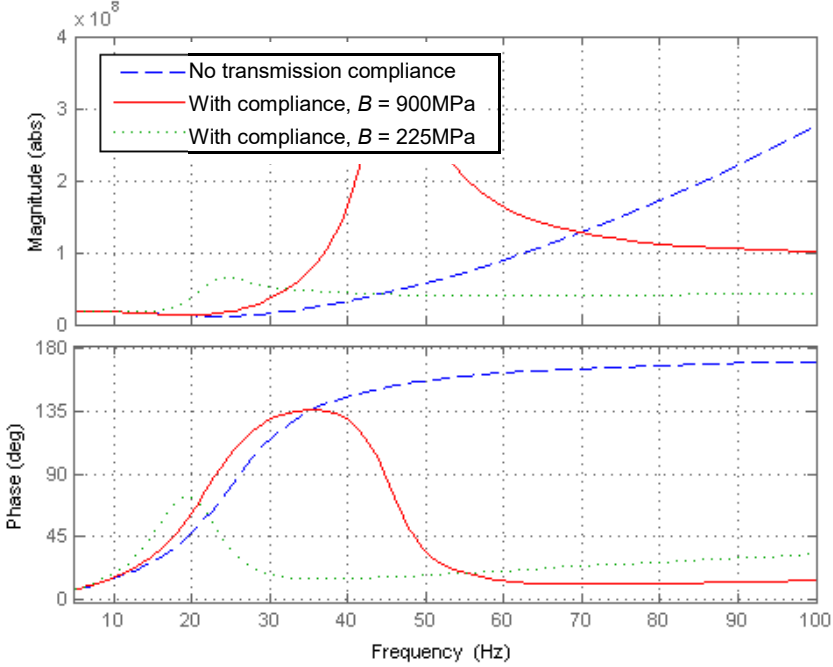


Figure 7. Predicted passive transmitted force per displacement transfer function (N/m)

### 3 EXPERIMENTAL PROTOTYPE

#### 3.1 Prototype design

An experimental prototype has been design and constructed. This has a bi-directional gear pump integrated with the housing of a brushless DC motor forming one pressure vessel, so that the permanent magnet rotor runs in hydraulic fluid. As no shaft seal is required for the pump, the case pressure can be raised to a high value (80 bar in this case), which becomes the mean system pressure about which large pressure deviations can occur without the danger of cavitation. The motor angular position is measured by a resolver, which provides high accuracy as well as reliable operation submerged in hydraulic oil. The pump is connected to a short stroke double-ended cylinder, which bears against a 7.9 mm thick stainless steel flex plate. This acts as the stiff spring in parallel with the hydraulic cylinder, taking the place of the composite strut in the helicopter. Figure 8 shows a cutaway drawing of the Resonant EHA, and Figure 9 shows the unit mounted in a testing machine. Figure 10 shows the motor design in more detail; note that the gear pump acts as the lower bearing for the permanent magnet rotor. A list of bought-in components is given in Table 2

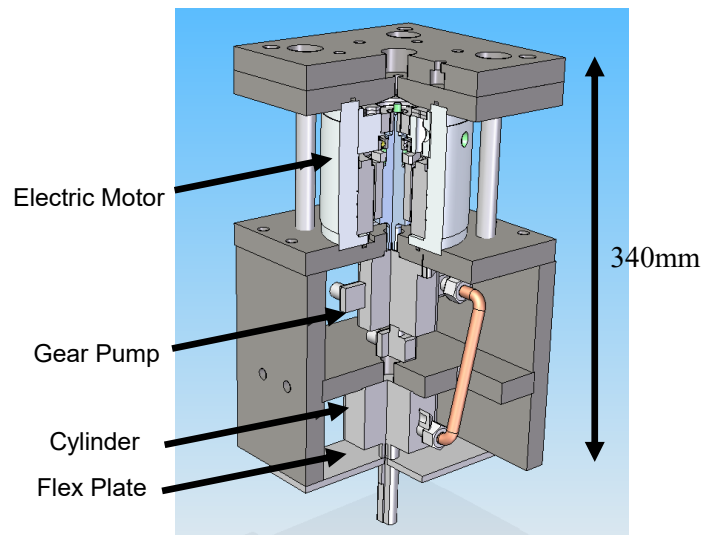


Figure 8. Sectioned drawing of Resonant EHA prototype

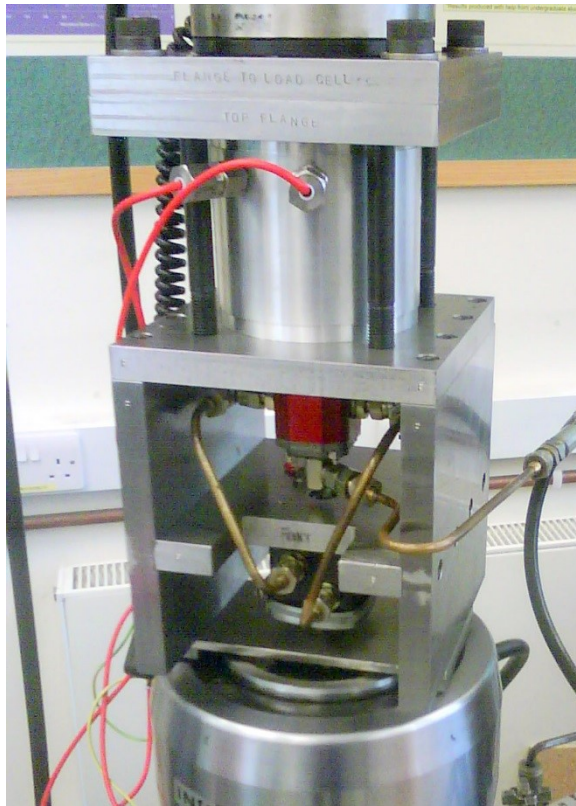


Figure 9. Prototype Resonant EHA mounted in test machine

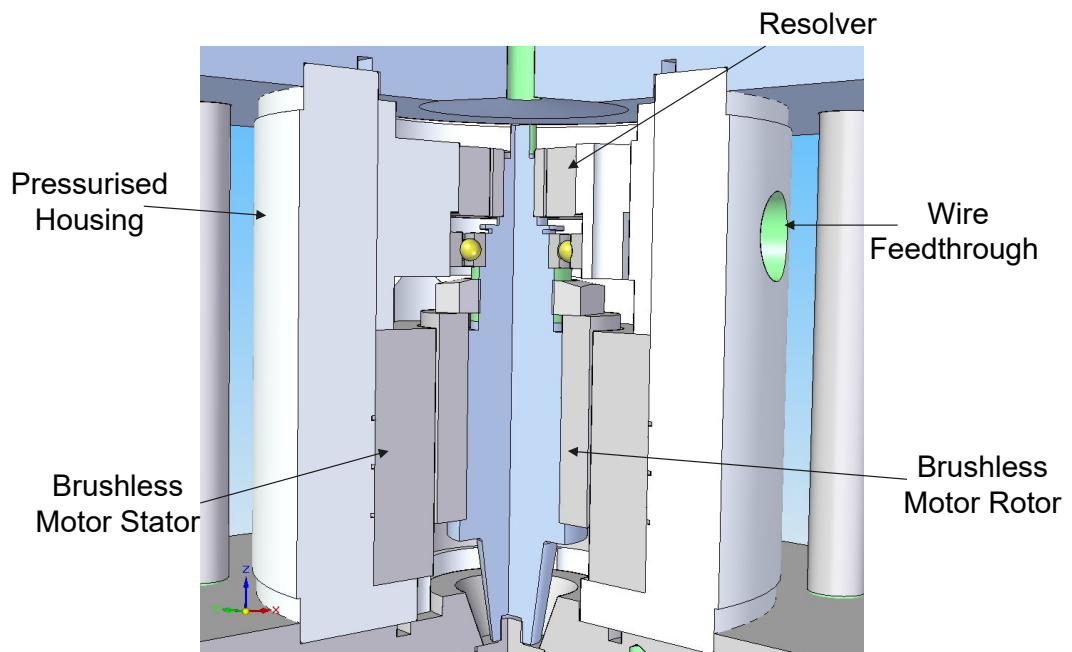


Figure 10 Brushless DC motor arrangement

A flexible hose is attached to the case drain port of the pump, adding some hydraulic compliance, effectively fulfilling the role of a small accumulator. Pumping fluid into the hose was used to charge the system up to the required mean pressure. Variation in mean pressure during operation due to external leakage or thermal expansion was found to be negligible. Two 200 bar pressure sensors are attached via T-junctions between the cylinder and the pump ports. The hydraulic circuit diagram, Figure 4, shows pressure relief valves that were not included in the proof-of-concept prototype.

Table 2 Main bought-in components

Component	Description
Kollmorgen KBMS 17x01C frameless brushless DC electric motor.	6 Nm peak, 2.1 Nm continuous torque, 810 W continuous power, 1 kg stator and rotor mass.
Harowe 15BRCX-601-K10 resolver.	$\pm 10$ arcmin resolution.
Kollmorgen AKD 01206 servo drive.	240 V DC voltage bus
TC Ltd. WFS-1/2"BSPT-18CU-3-V and WFS-1/4"NPT-24CU-4-V wire feedthroughs.	Multiple wire sealing assembly for pressure vessels.
Vivoil XV-0R 11 01 B BB E hydraulic gear motor.	1.5 cm <sup>3</sup> /rev displacement, external case drain.
Parker 32 K T CHD hydraulic cylinder.	Compact mounting, 36 mm diameter bore, 18 mm diameter double ended rod, 10 mm stroke.

### 3.2 Test setup and control scheme

The Resonant EHA is mounted in an Instron 1332 servohydraulic dynamic materials testing machine where the mechanical excitation is from below and an Instron 2518-101 load cell measures the transmitted force to the test machine frame. Two open loop demand channels, the servo motor demand (typically a torque input, with velocity or displacement inputs possible) and the testing machine demand (typically a displacement input, with a force input possible) are generated by a single waveform card with a common clock. In addition to these two demand channels, the following six channels of data are synchronously recorded:

- 1 Load cell force.
- 2 Pressure  $P_1$  (positive pressure extends cylinder rod).
- 3 Pressure  $P_2$  (positive pressure retracts cylinder rod).



- 4 Resolver motor angular position.
- 5 Displacement of testing machine (LVDT).
- 6 Cylinder extension (LVDT), measured between flex plate and hydraulic cylinder.

The current feedback and velocity feedback from the electric motor can also be recorded separately. A thermistor is present within the electric motor. The thermistor output is monitored by the servo drive which cuts out in the occurrence of an over temperature event. The temperature of fluid next to the electric motor is separately measured by a thermocouple which can be monitored visually. A schematic of the signals in the test setup is shown in Figure 11.

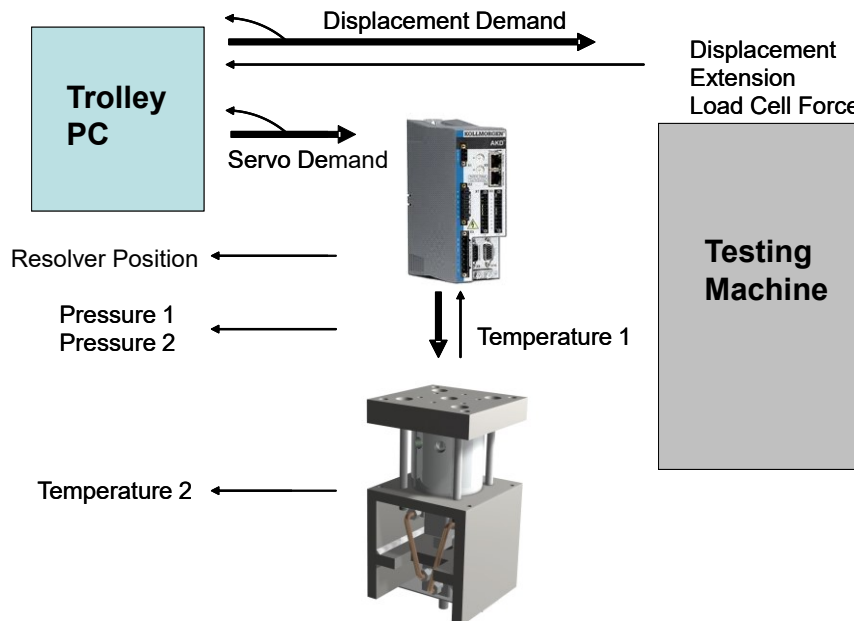


Figure 11 Diagram of signal paths in experimental system

### 3.3 EHA prototype characterisation

#### Flex Plate

A series of specific tests was undertaken to verify component parameter values. The flex plate was experimentally found to have a stiffness of 14.6 kN/mm, giving a theoretical resonant frequency of 22.4 Hz. **Error! Reference source not found.** shows the predicted deflection of the flex plate using Finite Element Analysis (FEA), in which the boundary conditions are rigid clamping at both ends. A 7kN force is applied, distributed around the inner surface of the centre

hole. The contour lines indicate deflection magnitude, the maximum deflection being 0.38mm at the centre hole (see [14] for more details). The experimentally measured stiffness is about 20% lower than that given by FEA, probably due to bending at the clamped ends.

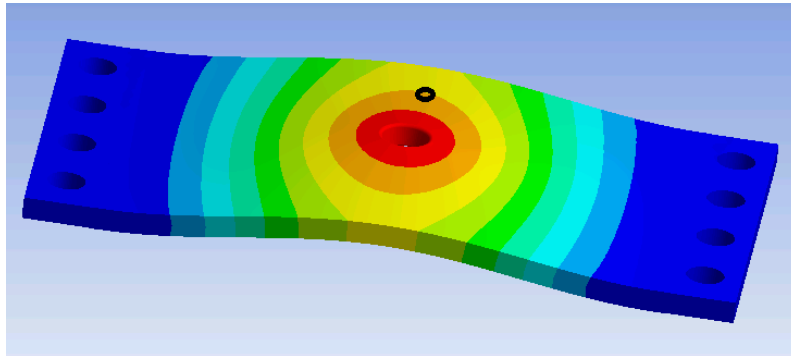


Figure 12 FEA visualisation of flex plate deflection

### **Rotor inertia**

The inertia of the motor rotor, including the hydraulic pump inertia, was estimated by demanding a sinusoidal angular velocity (157 rad/s amplitude, 20 Hz frequency) with the rotor in air, and by measuring the peak current required to obtain the peak acceleration. Relating the estimated torque to angular acceleration gave a rotor inertia of 1.40 kgcm<sup>2</sup>. This rotor inertia is close to the value predicted from CAD modelling and manufacturer's data.

### **Motor-pump friction**

The combined viscous drag of the PM rotor and the friction in the hydraulic pump was investigated by moving the cylinder using the testing machine with a 0.1 Hz to 0.5 Hz range of 3mm amplitude triangular waves in position control. The pressure difference across the gear pump and the rotor velocity were recorded. The frictional torque was calculated from the product of pump displacement and pressure difference with the results shown in Figure 13. Coulomb friction dominated the viscous friction components for the velocities tested. The offset in torque resistance with direction is attributed to the initial pump running-in being performed in only one direction. A combined pump and rotor friction model was used in the simulation where a Coulomb friction model was implemented for the gear pump, and a viscous friction model used for the rotor. The Coulomb friction values of -120 mNm and 60 mNm absolute values were chosen and combined with the viscous torque of 0.7 mNms/rad; this friction model is plotted in the Figure.

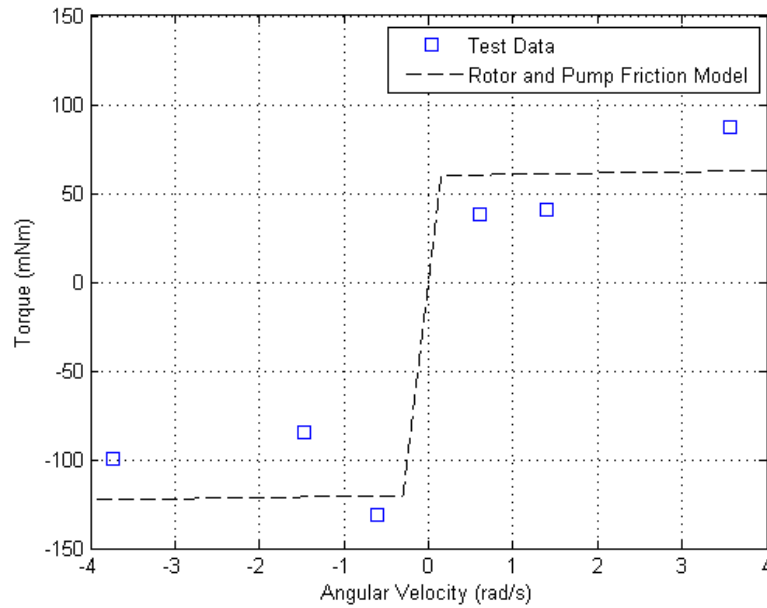


Figure 13 Frictional torque resistance against rotor velocity for gear pump and motor. Dashed line shows Coulomb and viscous friction model.

### Cylinder Seal Friction

The cylinder and gear pump friction (with the electric motor rotor not present) were tested by using the test machine to impose a 0.35 mm amplitude triangle wave at 20 Hz (Figure 14). The average friction magnitude was 760 N. Similar friction values results were found for other displacement inputs. Subtracting the gear pump friction found previously, gives a cylinder seal Coulomb friction value of 550N. Note that the combined seal and gear pump friction showed variability even with nominally identical tests.

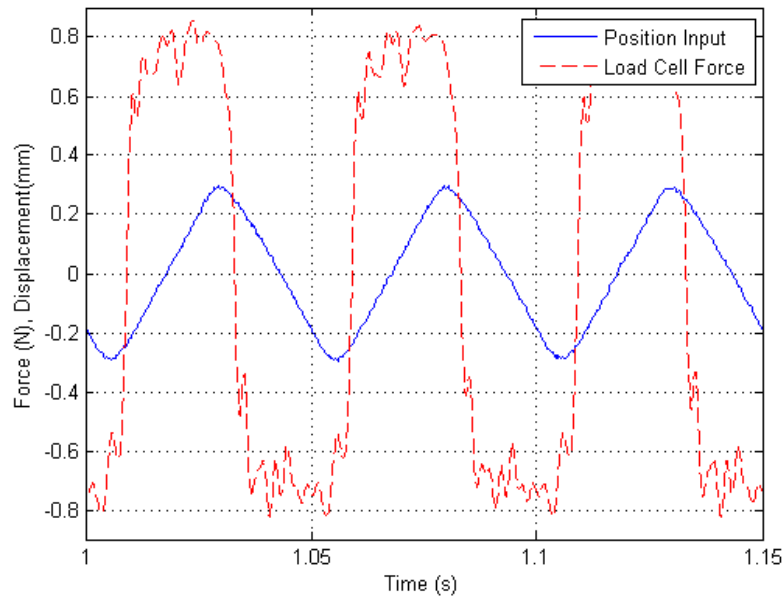


Figure 14 Friction from the hydraulic cylinder and gear pump (70 bar system pressure).

### Pump Internal Leakage

The internal leakage of the gear pump was found by driving it with a constant torque against blocked ports and measuring the pressure difference and quasi steady state angular velocity which resulted. The leakage was found for a positive pressure difference ( $P_1 - P_2$ ) to be  $1.0 \times 10^{-13}$   $\text{m}^3/\text{s}/\text{Pa}$ , and for a negative pressure difference to be  $1.8 \times 10^{-13}$   $\text{m}^3/\text{s}/\text{Pa}$ . The leakage magnitude is similar to those given in previous literature [15]. The difference in leakage values with direction may be attributed to the initial pump running-in being performed in only one direction.

### Stiffness Characterisation

The stiffness of the fluid and mechanically compliant elements (such as seals) can be found from the angular change of the pump shaft to torque square wave inputs when the cylinder position is locked, or with pump ports blocked to characterise the pump alone. The rotation for a 1 Hz bi-directional torque square wave input of different amplitudes is shown in Figure 15 for blocked ports. Superimposed on the drift due to leakage is a ripple caused by tooth engagement and disengagement. The jumps in position, of about  $40^\circ$ , coinciding with torque reversals, are thought to be as a result of a momentary loss of fluid past the meshing teeth during torque reversal. To

avoid this backlash-like effect, a mean torque is used to preload the EHA and avoid torque reversals during vibration testing. The equivalent plot with a uni-direction torque is shown in Figure 16. This gives a maximum angle change on torque reversal of  $8^\circ$ , reducing with torque amplitude, which can be explained by conventional hydraulic compressibility effects. The effective bulk modulus for the system was estimated to be 700 MPa [14].

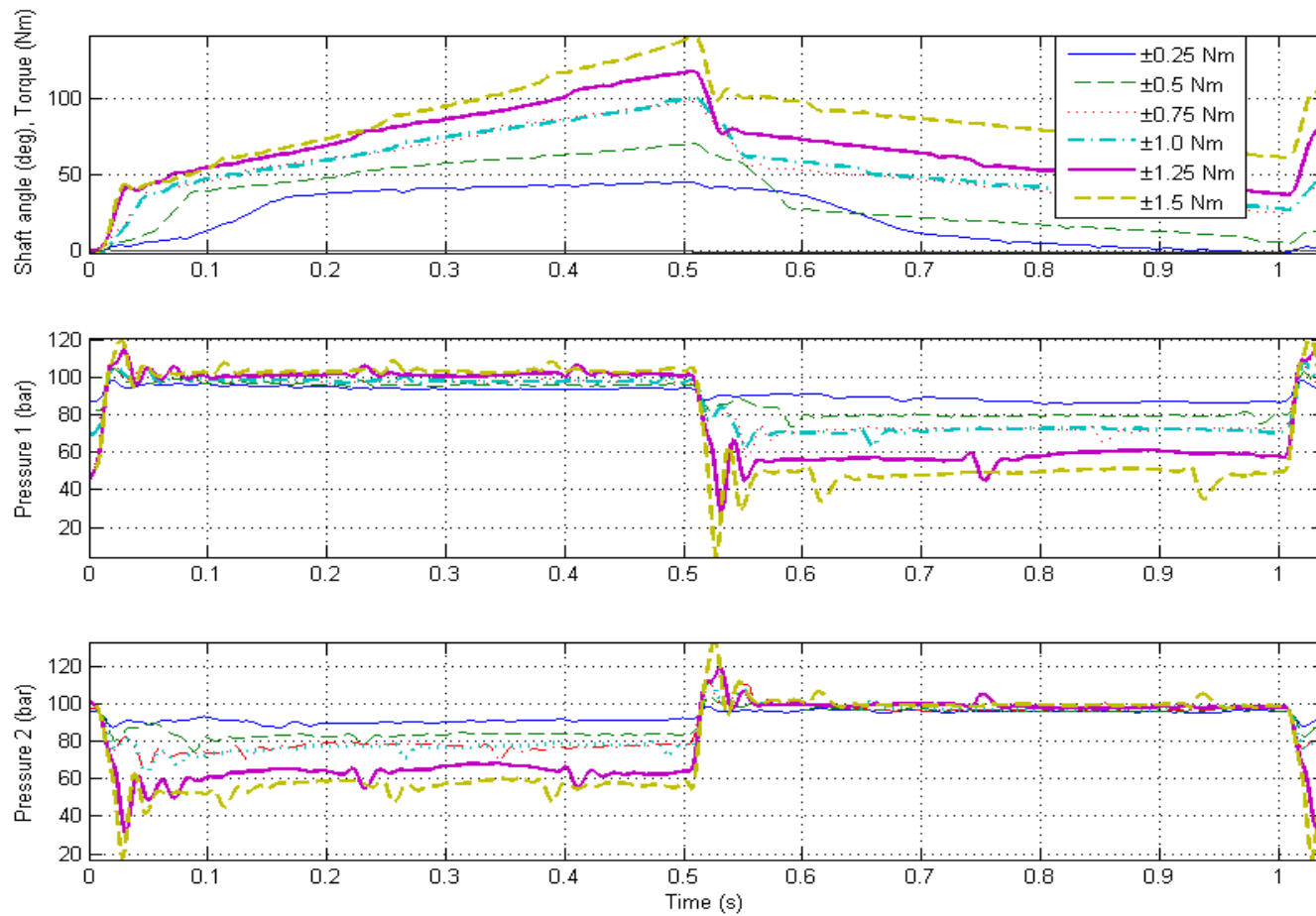


Figure 15 Motor rotor position and pressures for square wave  $\pm 0.25$  Nm to  $\pm 1.5$  Nm torque inputs with blocked pump ports.

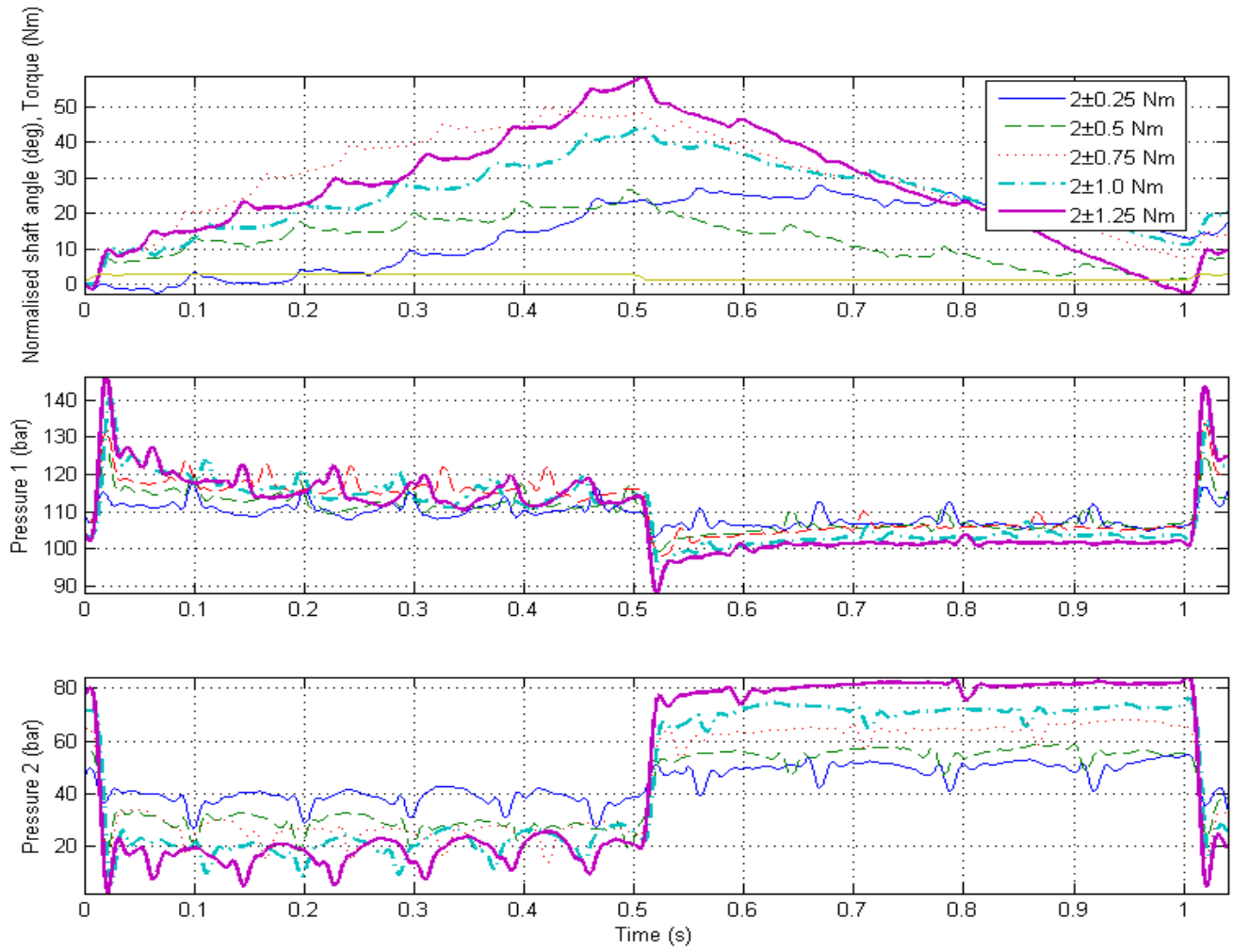


Figure 16 Motor rotor position and pressures for square wave  $2 \pm 0.25$  Nm to  $2 \pm 1.25$  Nm torque inputs against blocked ports. The changes in mean position have been subtracted for comparison purposes.

#### 4. SIMULATION MODEL

A non-linear simulation model of the prototype Resonant EHA has been constructed. The modelling of each part of the EHA is described in this section.

The torque of the brushless DC motor and pump are considered first. The motor current was controlled to provide a direct way of adjusting torque. The output torque of the motor is given by equation (15), and can be related to the differential pressure across the pump by equation (16):

$$T = K_t i - I \omega - T_f \quad (15)$$

$$T = D(P_1 - P_2) \quad (16)$$

where  $i$  is the current input,  $K_t$  is the torque constant,  $I$  is the combined inertia of motor, shaft coupling and pump,  $\omega$  is the rotational speed of the motor, and  $T_f$  is the frictional torque acting on the motor and pump. The inertias are combined as they have been measured together, and likewise the frictional losses, hence there is no frictional torque loss included in equation 16.

The motor-pump frictional torque depends on angular velocity with Coulomb and viscous components (model shown in Figure 13):

$$T_f = \begin{cases} T_{+C} + c_{Sh}\omega & \text{if } c_{Mf}\omega \geq T_{+C} \\ c_{Mf}\omega & \text{otherwise} \\ -T_{-C} + c_{Sh}\omega & \text{if } c_{Mf}\omega \leq -T_{-C} \end{cases} \quad (17)$$

where  $T_{+C}$  and  $T_{-C}$  are Coulomb friction torques in each direction,  $c_{Sh}$  is the combined viscous friction coefficient, and  $c_{Mf}$  is a transitional friction coefficient close to zero velocity.

With reference to Figure 17, the flow equations for fluid in lines either side of a hydraulic pump are:

$$Q_1 = D\omega - K_{II}(P_1 - P_2) - K_{EI}(P_1 - P_{Ac}) \quad (18)$$

$$Q_2 = D\omega - K_{II}(P_1 - P_2) + K_{EI}(P_2 - P_{Ac}) \quad (19)$$



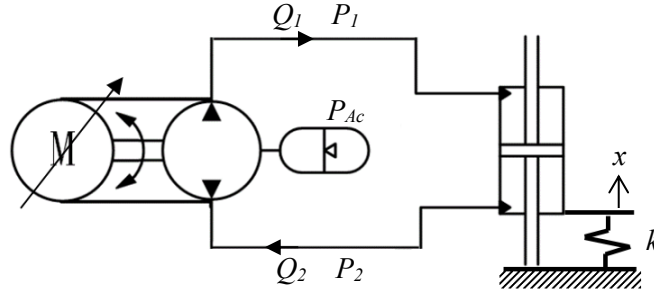


Figure 17 Annotated circuit diagram

where  $K_{Il}$  is the internal leakage coefficient of the pump,  $K_{El}$  is the external leakage coefficient of the pump,  $P_1$  and  $P_2$  are the pressures in each line,  $P_{Ac}$  is the accumulator pressure.

Accumulation is provided by a flexible hose filled with hydraulic fluid and is modelled as:

$$\dot{P}_{Ac} = \frac{Q_{El} B_{Ef}}{V_{Ho}} \quad (20)$$

where  $B_{Ef}$  is the effective bulk modulus of the fluid in a flexible hose and  $V_{Ho}$  is the volume of the hose.  $Q_{El}$  is the external leakage flow of the pump into the hose, given by:

$$Q_{El} = K_{El}(P_1 - P_{Ac}) + K_{El}(P_2 - P_{Ac}) \quad (21)$$

The flow equations of fluid into and out of a double ended actuator are:

$$Q_1 = A_1 \dot{x} + \frac{V_{1i} + Ax}{B} \dot{P}_1 + K_{Lc}(P_1 - P_2) \quad (22)$$

$$Q_2 = A_2 \dot{x} - \frac{V_{2i} - Ax}{B} \dot{P}_2 + K_{Lc}(P_1 - P_2) \quad (23)$$

where  $x$  and  $\dot{x}$  are the displacement and velocity of the piston which is rigidly connected to the gearbox,  $B$  is the bulk modulus of the oil,  $K_{Lc}$  is the internal leakage coefficient of the piston,  $V_{1i}$  and  $V_{2i}$  are the initial volume of chamber 1 and 2 plus fluid in the connecting pipes respectively. The EHA output force is given by:

$$F_{EHA} = A(P_1 - P_2) - F_f \quad (24)$$

where  $F_f$  is a friction force acting on the piston which is either of the three states:

$$F_f = \begin{cases} F_C & \text{if } c_{Cf} \dot{x} \geq F_C \\ c_{Cf} \dot{x} & \text{otherwise} \\ -F_C & \text{if } c_{Cf} \dot{x} \leq -F_C \end{cases} \quad (25)$$

where  $F_C$  is the maximum Coulomb friction and  $c_{Cf}$  is a transitional friction coefficient.

The EHA acts in parallel with the flex plate of stiffness  $k$ , giving a spring force of:

$$F_{Sp} = kx \quad (26)$$

The net force which should be minimised for optimum vibration isolation is:

$$F_{Ne} = kx - F_{EHA}(\dot{x}) \quad (27)$$

These modelling equations are used to simulate the Resonant EHA using Simulink. Simulation results are shown in comparison with experiment in the next section. Parameters values used in the simulation model are summarised in Table 3.

Table 3 Parameter values

Parameter	Value
Strut stiffness, $k$	14.6 kN/mm
Piston area, $A$	550 mm <sup>2</sup>
Motor displacement, $D$	1.52 cm <sup>3</sup> /rev
Combined inertia, $I$	1.4x10 <sup>-4</sup> kgm <sup>2</sup>
Torque constant, $K_t$	0.355 Nm/A
Viscous friction of motor and pump, $c_{sh}$	2 mNm/(rad/s)
Internal leakage coefficient of pump, $K_{I1}$	1.0x10 <sup>-13</sup> m <sup>3</sup> /Pa
Internal leakage coefficient of pump, $K_{I2}$	1.8x10 <sup>-13</sup> m <sup>3</sup> /Pa
External leakage coefficient of pump, $K_{E1}$	1.0x10 <sup>-13</sup> m <sup>3</sup> /Pa
System pressure, $P_{Ac}$	80 bar
Nominal bulk modulus, $B$	700 MPa
Pump absolute friction positive direction, $T_{+C}$	60 mNm
Pump absolute friction negative direction, $T_{-C}$	120 mNm
Hose (accumulator) volume, $V_{Ho}$	55 cm <sup>3</sup>
Hose effective bulk modulus, $B_{Ho}$	180 MPa
Internal leakage coefficient of cylinder, $K_{Lc}$	1.0x10 <sup>-11</sup> m <sup>3</sup> /s/Pa
Initial volume of each chamber and connection, $V_{1i}$ , $V_{2i}$	8.9 cm <sup>3</sup>
Cylinder Coulomb friction value, $F_C$	550 N

## 5 EXPERIMENTAL RESULTS

All active and passive testing was carried out using a 0.18 mm amplitude sinusoid displacement input, and a 1Nm mean torque to preload the EHA. Passive testing was undertaken with the motor electrically open-circuit. An example of measured pressures and force with a 20Hz displacement input are shown in Figures 18 and 19. The measurements are compared with simulation results from the model described in Section 4, showing a reasonably good match.

Estimating the transmitted force from this Figure and a range of other frequencies gives the plot in Figure 20, where the force is normalised by the displacement amplitude to give an ‘apparent stiffness’. In Figure 20, “RMS” uses the root mean square average of the load cell force, i.e. including all frequency components in the net force waveform, while “Fundamental” uses the RMS of the component at the excitation frequency alone. The passive attenuation of the transmitted force is demonstrated, with a 40% force reduction at 20Hz (the resonant frequency) in comparison with 5Hz. Although there are some discrepancy between simulation and experimental results, particularly above the resonant frequency, the simulation predicts the trends reasonably well.

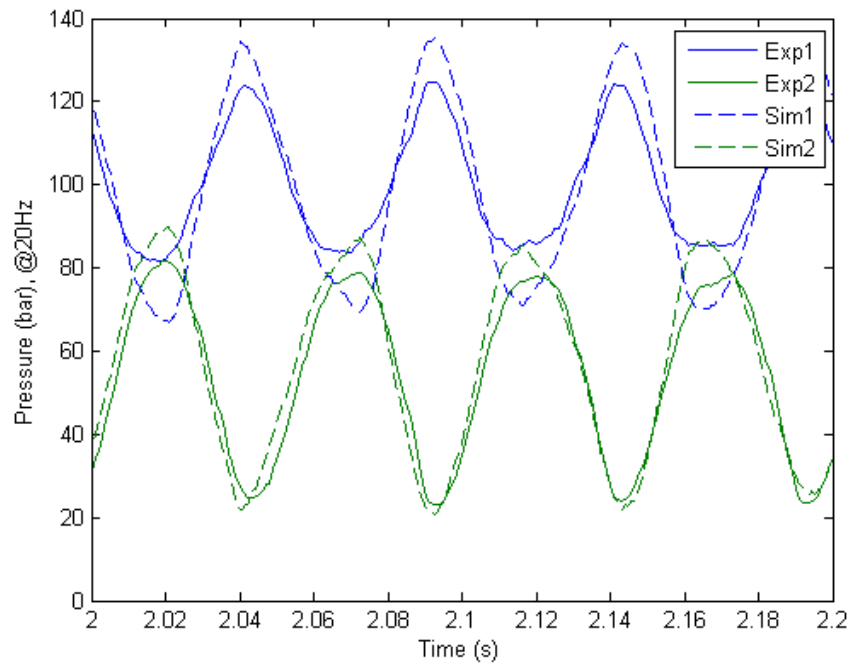


Figure 18 Experimental and simulated pressures,  $P_1$  and  $P_2$ , at 20 Hz.

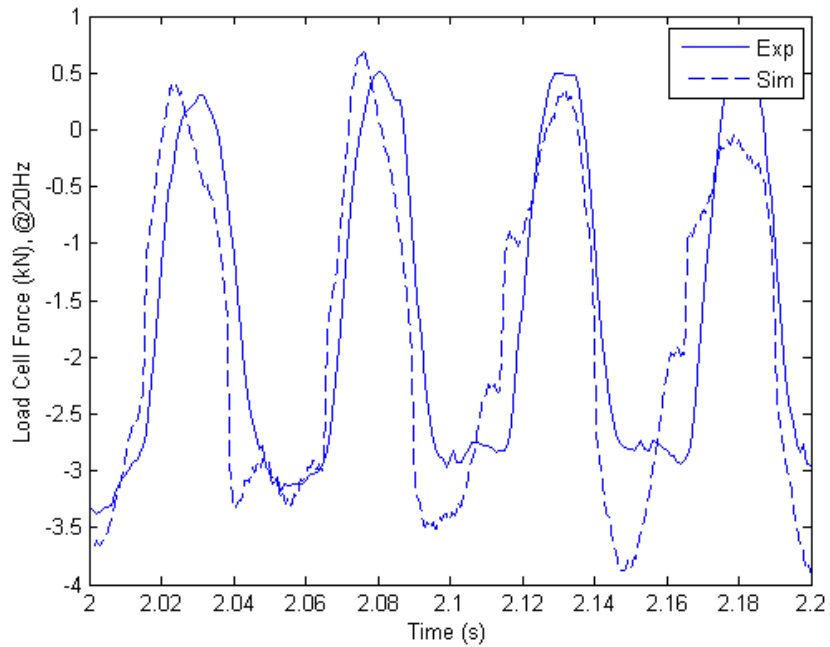


Figure 19 Experimental and simulated net forces at 20 Hz

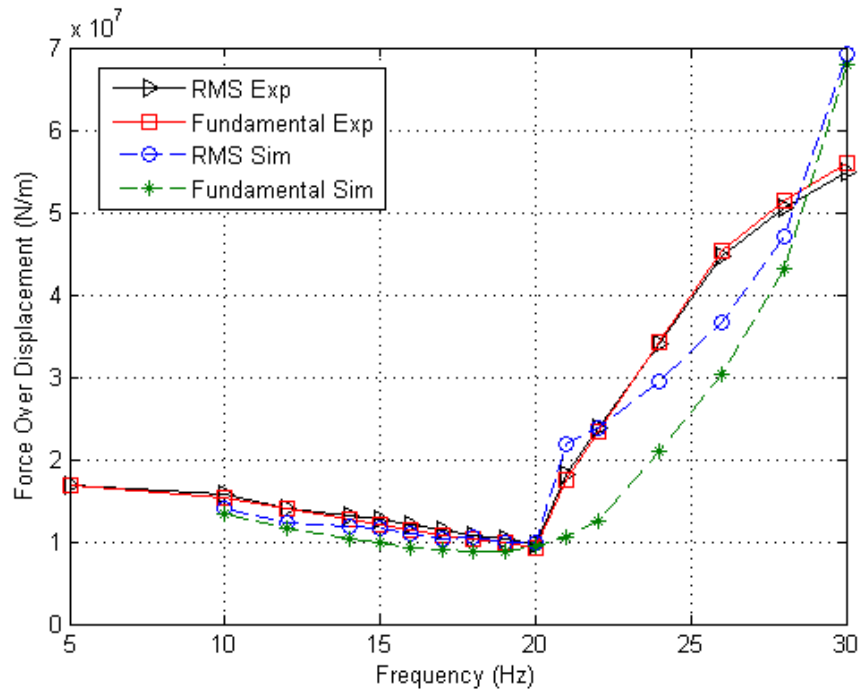


Figure 20 Passive experimental and simulated net apparent stiffness

For active vibration control, the electric motor was used in current control, effectively controlling torque, with a sinusoidal demand. For each displacement input frequency, the same torque demand frequency was used. The amplitude and phase of the demand was varied at each frequency until a minimum net load force was found. The net force results over the range 5 Hz to 30 Hz are shown in Figure 21. Active torque control significantly lowers the transmitted force. ‘Baseline’ is the behaviour for the flex plate spring alone, based on its measured stiffness and an estimated small damping term. The torque amplitudes required to obtain a minimum net force at 10 Hz and 20 Hz are given in Table 4, showing that the simulation predicts the required torques quite well.

Table 4 Dynamic torque amplitude for minimum net force.

Frequency (Hz)	Torque amplitude, Experiment (Nm)	Torque amplitude, Simulation (Nm)
10	0.98	1.04
20	0.57	0.64

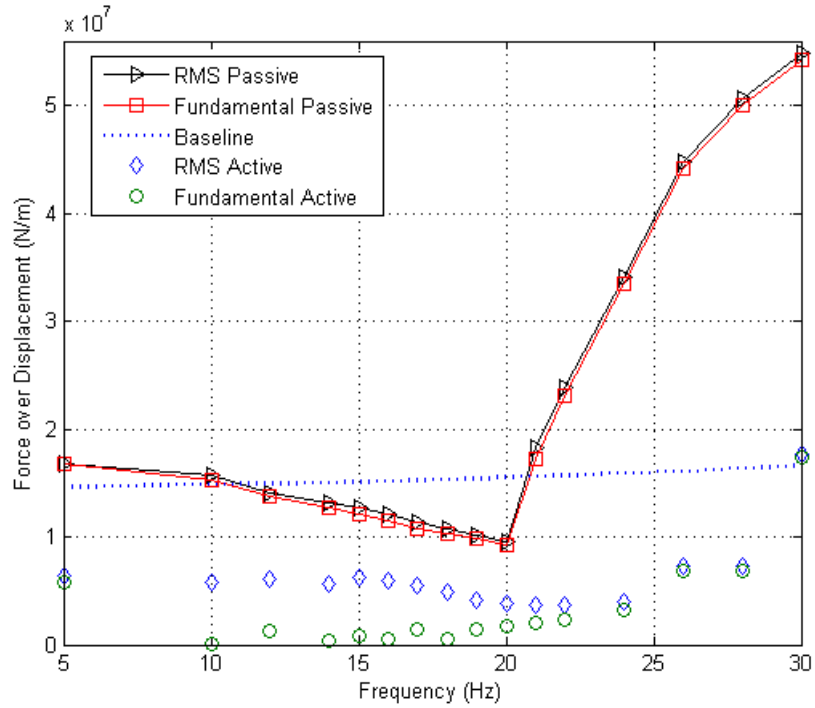


Figure 21. Experimental apparent stiffness with active augmentation.

## 6 CONCLUSIONS

A novel electro-hydrostatic actuator (EHA) intended for active vibration isolation has been conceived, developed and investigated. Passively, the reflected inertia of the rotary components in the EHA forms what is sometimes termed an inerter, and provides a degree of passive vibration isolation at the dominant frequency. Active control of the motor extends the isolation performance of the passive device by compensating for losses, and also broadens the frequency of isolation away from the resonant frequency. There are significant advantages of the approach over conventional methods:

- a wider range of operating frequencies and better isolation performance than a purely passive system,
- lower power consumption than a purely active system, which also results in a smaller and lighter unit,
- the local hydraulic transmission in the EHA proves a more robust and longer lasting solution than a mechanical transmission due insensitivity to vibration-related wear,

- the EHA can be protected against shock loading by incorporating cross-line relief valves
- power is supplied electrically rather than hydraulically.

The latter point is one of the main factors in the motivating application, which is isolating the vibration of the rotor hub from the fuselage in rotorcraft. This allows use of active vibration isolation on future helicopters with limited or no hydraulic power availability. Further, a resonant EHA could improve isolation performance in other applications, such as vehicle suspension systems or mountings for large engines (e.g. in ships).

From the results in Figure 21, it can be seen the Resonant EHA as a hybrid active-passive isolator achieved reduction of up to a factor of four in RMS force transmission against the baseline strut and near complete cancellation at the fundamental frequency from 10 Hz to 20 Hz. At 20 Hz a dynamic torque of 0.57 Nm was experimentally required to achieve the force over displacement magnitude shown. This is half the theoretical 1.15 Nm that would be required from an equivalent loss-free purely active system. Considering that the 0.57 Nm dynamic torque is also compensating the relatively high cylinder friction in the experimental system and real losses in the pump the actively augmented vibration suppression system performs well.

The concept has been patented prior to commercial exploitation, and as has been demonstrated marks a major advance of conventional passive or active vibration isolation methods.

## **ACKNOWLEDGEMENTS**

The project was funded by the University of Bath, Great Western Research, and AgustaWestland Ltd. Patent application GB1112244.7 which describes the Resonant EHA device has been assigned to the project industrial partner, AgustaWestland Ltd. (now Leonardo Helicopters).

## **References**

1. R. Navarro, (1997) "Performance of an Electro-Hydrostatic Actuator on the F-18 Systems Research Aircraft," Report NASA/TM-97-206224.
2. M. Todeschi, (2007) "A380 flight control actuation - Lessons learned on EHAs design," presented at the Recent Advances in Aerospace Actuation Systems and Components, Insa Toulouse, 2007.
3. K. G. Cleasby and A. R. Plummer, (2008) "A novel high efficiency electro-hydrostatic flight simulator motion system," Fluid Power Motion Control (FPMC2008), Bath, UK Sept 2008.

4. Pearson, J. T., Goodall, R. M., & Lyndon, I. (1994). « Active control of helicopter vibration. » *Computing & Control Engineering Journal* (December), 277-284.
5. Jiang, J. Z., Smith, M. C., & Houghton, N. E. (2008). "Experimental testing and modelling of a mechanical steering compensator. " Paper presented at the ISCCSP, Malta.
6. Stamps, F. B., & Smith, M. R. (1997). U.S. Pat. No. 6009983.
7. P. Konstanzer, B. Enekl, P.-A. Aubourg, and P. Cranga, (2008) "Recent advances in Eurocopter's passive and active vibration control," presented at the American Helicopter Society 64th Annual Forum, Montreal, Canada, 2008.
8. Kryszinski, T., & Malburet, F. (2007). "Mechanical Vibrations: Active and Passive Control. London". ISTE.
9. Flint, E., Evert, M., Anderson, E., & Flannery, P. (2000). "Active/passive counter-force vibration control and isolation systems". Paper presented at the IEEE 2000 Aerospace Conference, Montana, USA.
10. Daley, S., Zazas, I., & Hatonen, J. (2008). "Harmonic control of a 'smart spring ' machinery vibration isolation system. " *Proc Instn Mech Engrs, Part M: Journal of Engineering for the Maritime Environment*, 222.
11. Yu, Y., Naganathan, N. G., & Dukkipati, R. V. (2001). "A literature review of automotive vehicle engine mounting systems". *Mechanism and Machine Theory*, 36, 123-142.
12. Mansour, H., Arzanpour, S., & Golnaraghi, F. (2011). "Design of a solenoid valve based active engine mount". *Journal of Sound and Vibration*
13. Chen MQ, Hu Y, Li C, Chen G. (2016) "Application of Semi-Active Inerter in Semi-Active Suspensions Via Force Tracking. " *ASME. J. Vib. Acoust.*;138(4).
14. Henderson, J-P. (2012) "Vibration Isolation for Rotorcraft Using Electrical Actuation". PhD Thesis, University of Bath, UK
15. R. Kang, Z. Jiao, S. Wu, Y. Shang, and J.-C. Mare, (2008) "The nonlinear accuracy model of electro-hydrostatic actuator," presented at the IEEE Conference on Robotic, Automation and Mechatronics, 2008.